

Numerical modeling of plant root controls on gravel bed river morphodynamics

Journal Article

Author(s):

Caponi, Francesco ; Siviglia, Annunziato 

Publication date:

2018-09-16

Permanent link:

<https://doi.org/10.3929/ethz-b-000293837>

Rights / license:

[In Copyright - Non-Commercial Use Permitted](#)

Originally published in:

Geophysical Research Letters 45(17), <https://doi.org/10.1029/2018GL078696>

Funding acknowledgement:

159813 - Eco-morphodynamic modelling for gravel bed rivers (SNF)

Numerical modeling of plant-root controls on gravel-bed river morphodynamics

F. Caponi ¹ and A. Saviglia ¹

¹Laboratory of Hydraulics, Hydrology and Glaciology, ETH Zurich, Switzerland

Key Points:

- A model accounting for the biogeomorphic feedbacks between plant roots and riverbed morphodynamics is presented
- Uprooting is the primary plant-root biogeomorphic feedback controlling the co-evolution of gravel-bed river morphodynamics and vegetation
- The competition between the potential flow erosion and the uprooting depth mediates plant-root controls on riverbed morphodynamics

Abstract

The role of vegetation in shaping the geomorphology of rivers, deltas, along with tidal and estuarine environments is widely recognized. While mutual interactions between flow, plant canopy and morphodynamics have been extensively investigated, similar studies considering plant roots are limited. Here, we present results from numerical model that quantify the feedbacks of both the above- and below-ground vegetation on gravel-bed river (GBR) morphodynamics. Plant-root biogeomorphic feedbacks, i.e. uprooting and root-enhanced riverbed cohesion, are quantified through the description of the vertical root distribution. By investigating the evolution of the riverbed of a straight gravel channel with a vegetated patch, we show that uprooting is the primary plant-root biogeomorphic feedback determining the evolution of the riverbed and the competing influence of the potential flow erosion versus uprooting depth mediates the plant-root controls on morphodynamics. These findings broaden our understanding on the role played by plant roots on GBR morphodynamics.

1 Introduction

The role of vegetation in shaping the geomorphology of interfaces between water and land surfaces, such as river bars and floodplain, river deltas, along with tidal and estuarine environments, is widely recognized [Corenblit *et al.*, 2015]. Mutual interactions among riparian vegetation, water flow and sediment transport result in a series of biogeomorphic feedbacks [sensu Corenblit *et al.*, 2007] that can affect bar and landform formation in vegetated rivers [e.g. Gurnell, 2014; Bertoldi *et al.*, 2011], determine shifts among alternate stable states [Bertoldi *et al.*, 2014; Bertagni *et al.*, 2018], shape river deltaic marshes [Nardin and Edmonds, 2014] and promote formation of drainage channel networks in tidal systems in the presence of marshes [e.g. Temmerman *et al.*, 2007; Schwarz *et al.*, 2018]. Consequently, development of eco-morphodynamic numerical models [Murray and Paola, 2003; Bertoldi *et al.*, 2014; Oorschot *et al.*, 2016], which quantify such feedbacks, is crucial for predicting the morphodynamics of these areas and for planning sustainable restoration and flood mitigation measures [Wohl *et al.*, 2015].

Although the general importance of vegetation is widely recognized, its precise role in mediating biogeomorphic feedbacks in rivers is not clear. A number of studies indicate that the emergence and strength of vegetation-related feedbacks result from the balance between physical and biological processes [e.g. Corenblit *et al.*, 2007; Tal and Paola, 2007].

Modification of sediment supply rates has been suggested as a mechanism responsible for muting the effects of species-specific plant traits on morphodynamics of sand-bed rivers [Manners *et al.*, 2015; Diehl *et al.*, 2017] and for altering the vegetation's effects on channel dynamics in GBRs [Gran *et al.*, 2015]. Changes in the hydrological regime, including flood frequency and magnitude [Vesipa *et al.*, 2017], as well as water table fluctuations, have been argued to impact biogeomorphic succession and river channel morphodynamics [Bätz *et al.*, 2016; Bertoldi *et al.*, 2011; Bertagni *et al.*, 2018]. Subsurface flows and alteration of pore-water pressures in the hyporheic zone may also contribute to mediate the effects of vegetation on cohesive riverbeds [e.g. Simon and Collison, 2001; Cancienne *et al.*, 2008]. Among these processes, survival of riparian vegetation is significantly threatened by morphological changes, which cause uprooting and scour, limiting plant community expansion [Gurnell *et al.*, 2012].

Most studies examining biogeomorphic feedbacks consider only the above-ground component of vegetation. Plant canopy, for instance, is known to change turbulence structure [Nepf, 2012] and to significantly increase flow resistance [e.g. Västilä and Järvelä, 2014; Aberle and Järvelä, 2015]. The reduction of bottom shear stresses in vegetated areas alters sediment transport, thereby inducing local and reach-scale riverbed changes [Vargas-Luna *et al.*, 2015; Le Bouteiller and Venditti, 2015]. However, below-ground vegetation underpins fundamental biogeomorphic feedbacks that are often not included in these studies. Plant roots contribute to mediate riverbank cohesion and stability, shaping river planform styles [e.g. Tal and Paola, 2010; Pollen-Bankhead and Simon, 2010; Davies and Gibling, 2011; Gibling and Davies, 2012; Polvi *et al.*, 2014], promoting in-channel sediment stabilization and reducing scour [Pasquale *et al.*, 2012; Pasquale and Perona, 2014]. Roots provide resistance to the drag forces exerted by the flow on plant canopy, delaying or possibly avoiding uprooting [Edmaier *et al.*, 2011, 2015; Perona and Crouzy, 2018]. The amount of roots that anchor plants is of the utmost importance for determining the ability of vegetation to withstand erosional events [Bywater-Reyes *et al.*, 2015; Bankhead *et al.*, 2017]. Nonetheless, GBR morphodynamic models mainly describe the effects of roots on vegetation anchoring and scouring, adopting lumped approaches that are oversimplified [e.g. Murray and Paola, 2003; Bertoldi *et al.*, 2014].

Our goals are to present a simple modeling framework to study key biogeomorphic feedbacks of plant root and to show the results of model runs that test the importance of these feedbacks in predicting GBR morphology. We consider vegetation consisting of an

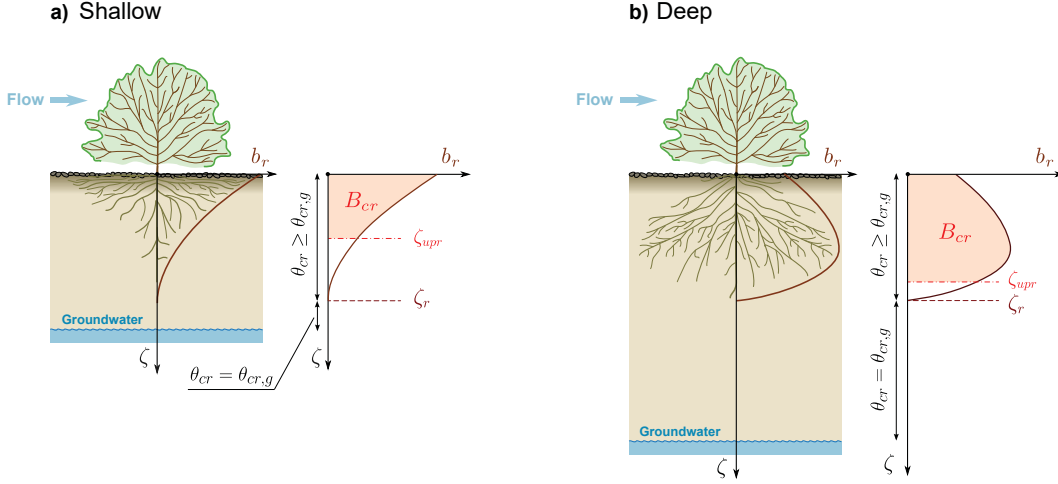


Figure 1. Vertical root density distributions b_r , (a) shallow and (b) deep, used to probe the role of uprooting and root-enhanced riverbed cohesion on the evolution of a GBR. B_{cr} is the fraction of the entire root biomass B_r that must be exposed to the flow before uprooting occurs, ζ_r the rooting depth, i.e. the depth to which the roots grow, and ζ_{upr} the uprooting depth. Further symbols are reported in the main text.

above- and below-ground component. We adopt the stochastic model developed by *Tron et al.* [2014] and characterize the plant roots by their vertical density distribution, which depends on water table dynamics. Then, we model plant-root biogeomorphic feedbacks depending on these distributions. This approach allows us to disentangle the role of the two vegetation components and to explore how plant root morphology influences biogeomorphic feedbacks. In this study, we examine a simplified GBR morphology, while retaining the key morphodynamic processes. We investigate the riverbed response to a vegetation patch in a straight gravel channel by varying hydromorphological configurations and vegetation characteristics.

2 Modeling Framework

2.1 Hydromorphodynamics

Hydromorphodynamic processes are simulated with the one-dimensional model BASEMENT [Vetsch *et al.*, 2017]. Firstly, the hydrodynamic problem is solved by integrating numerically the Saint-Venant equations and using the Manning-Strickler approach for the evaluation of the global flow resistance, whereby the total shear stress is evaluated

as

$$\tau = \frac{\rho g u |u|}{K_s^2 h^{1/3}} \quad , \quad (1)$$

where ρ is the water density, g is the gravitational acceleration, u is the vertically averaged flow velocity, h the water depth and K_s the Strickler coefficient. Secondly, the Exner equation is adopted to describe the time evolution of a cohesionless GBR composed of a uniform sediment. It reads:

$$(1 - p) \frac{\partial z_b}{\partial t} + \frac{\partial q_b}{\partial x} = 0 \quad , \quad (2)$$

where z_b is the bed elevation, p is the sediment porosity and q_b is the longitudinal bed-load flux. q_b is evaluated as a function of the excess of the Shields shear stress, θ , above a threshold value θ_{cr} , where

$$\theta = \frac{\tau}{(\rho_s - \rho) g d_s} \quad (3)$$

and ρ_s and d_s are the sediment density and diameter, respectively.

2.2 Plant Roots

Plant roots often display complex architectures [Gregory, 2008], with a maximum depth that is mostly limited by groundwater [Fan *et al.*, 2017] and a density that decreases with riverbed depth [Jackson *et al.*, 1996]. In riparian ecosystems, however, root growth tends to follow water table oscillations [Orellana *et al.*, 2012]. This is particularly relevant in GBRs where the large hydraulic conductivity in the hyporheic zone enhances exchanges between groundwater and stream flow [Cardenas *et al.*, 2004].

To describe the vertical root distribution, we adopt the stochastic model proposed by Tron *et al.* [2014], which describes root dynamics driven by water table oscillations. The model assumes that roots grow within an optimal zone whose fluctuations follow the water table oscillations, while roots decay otherwise (Figure S1). This zone results from the optimal balance between the amount of pore water available for root uptake and dissolved oxygen levels needed for root respiration [Gregory, 2008]. The maximum rooting depth is limited by the minimum depth reached by this optimal zone (see more details on the physical processes underlying the root model in the supporting information).

By considering water table fluctuations as a stochastic process [Ridolfi *et al.*, 2011], the model produces a probability density distribution (PDF) of the root density, b_r , over the riverbed depth, ζ , (downward oriented axis with origin at the riverbed, see Figures 1a, 1b and S1). This PDF depends on physically-based parameters that define the water table

oscillations (characterized by a mean oscillation depth, frequency and decay rate) and the plant root characteristics (see details on the mathematical formulation in the supporting information). In this study, we describe shallow root profiles (Figure 1a) that result from shallow and more variable water table oscillations and deep root profiles (Figure 1b) characterized by a deep and more stable water table [Tron *et al.*, 2014, 2015].

2.3 Biogeomorphic Feedbacks

2.3.1 Canopy feedback on flow resistance and sediment transport

The presence of plant canopy increases the global flow resistance by increasing local roughness, modifying flow patterns and providing additional drag [Nepf, 2012]. The additional drag varies significantly with morphology and bio-mechanical properties of canopy [Aberle and Järvelä, 2015], including stem density, flexibility, presence and type of foliage and submerged and emergent conditions [e.g. Västilä and Järvelä, 2014]. In line with previous models, which are based on a depth-averaged description of the flow [e.g. Bertoldi *et al.*, 2014], we model the global flow resistance (equation 1 to be used for hydrodynamic computation) by considering a single Strickler coefficient $K_{s,v}$ [Kim *et al.*, 2012; Bertoldi *et al.*, 2014; Le Bouteiller and Venditti, 2015] that incorporates not only the shear stress exerted by the fluid directly on the sediment grain (bottom shear stress), but also the additional drag generated by vegetation.

Flow pattern changes associated to the presence of vegetation have also profound effects on sediment transport [e.g. Yager and Schmeeckle, 2013; Le Bouteiller and Venditti, 2015]. Bottom shear stress is reduced in a plant patch, and the decrease is higher for denser vegetation [Le Bouteiller and Venditti, 2015] and larger plant frontal areas [Vargas-Luna *et al.*, 2015]. Since direct quantification of the bottom shear stress is extremely difficult in the presence of vegetation [Le Bouteiller and Venditti, 2015], we model the reduction of bottom shear stress by multiplying the total shear stress τ by a factor $\gamma \leq 1$ [Le Bouteiller and Venditti, 2015] and compute the sediment flux, q_b , using the reduced Shields stress, $\gamma\theta$.

2.3.2 Plant-root feedback on riverbed cohesion

Buried roots are known to significantly modify mechanical and biochemical properties of riverbed thereby reducing erosion on riverbanks and slope surfaces [Vannoppen

et al., 2015]. Studies assessing the reduced root-riverbed erosion in cohesive substrates often indicate a negative exponential relation between root density and the bed shear stress needed to mobilize sediments. However, this relation might not hold for cohesionless substrate, such as gravel, because of the different particle detachment mechanism [Politti *et al.*, 2018]. Alternatively, we can use a linear relation between root density (b_r) and the critical Shields parameter (θ_{cr}), as indicated by *Pasquale and Perona* [2014] for GBRs. We assume that at the riverbed depth ζ

$$\theta_{cr}(\zeta) = \theta_{cr,g} + (\theta_{cr,v} - \theta_{cr,g})b_r(\zeta), \quad (4)$$

where $\theta_{cr,g}$ and $\theta_{cr,v}$ ($> \theta_{cr,g}$) represent the threshold values for incipient sediment motion on bare and vegetated riverbed, respectively [Bertoldi *et al.*, 2014].

2.3.3 Uprooting

Plant removal by uprooting depends on the balance between drag forces of the water flow acting on the above-ground part of vegetation and resisting forces provided by the buried part of the roots [Edmaier *et al.*, 2011]. Resisting forces increase with rooting depth [Edmaier *et al.*, 2015; Bywater-Reyes *et al.*, 2015] and the maximum density depth [Pasquale *et al.*, 2012], most likely exceeding applied drag forces. Vegetation that develops substantial root biomass is, in fact, unlikely to be uprooted by drag forces alone even at high flows [Bywater-Reyes *et al.*, 2015; Bankhead *et al.*, 2017]. Uprooting rather occurs as a consequence of riverbed erosion that gradually exposes part of the roots to the flow thus reducing the anchoring resistance of the plant (Type II uprooting as defined by Edmaier *et al.* [2011]). Experimental evidence suggests that exposure of only part of the entire root biomass might be sufficient to uproot plants [Edmaier *et al.*, 2015]. In light of this evidence, we define a critical biomass value, B_{cr} , as the fraction β of the entire root biomass (Figure 1) that must be exposed to the flow before uprooting occurs. We calculate this value as follows:

$$B_{cr} = \beta \int_0^{\zeta_r} b_r(z) dz = \int_0^{\zeta_{upr}} b_r(z) dz, \quad (5)$$

and we assume that uprooting occurs when riverbed scouring reaches the uprooting depth ζ_{upr} . ζ_{upr} increases with the rooting depth (Figure S3) and depends on the value of β (Figure S2) and the root distribution (Figures 1a and 1b). Finally, when uprooting occurs b_r is set to 0 and $K_{s,v}$ to the Strickler value assigned to bare riverbed, $K_{s,g}$.

2.4 Numerical Simulations

Simulations are conducted under steady flow (constant discharge $Q = 100 \text{ m}^3/\text{s}$) in a straight rectangular channel of length $L = 1500 \text{ m}$, 10 m wide and initial constant slope S_0 . The bed is composed of uniform sediments ($p = 0.4$, reference grain size $d_s = 20 \text{ mm}$) and the bedload flux q_b is calculated using the Meyer-Peter and Müller formula [Meyer-Peter *et al.*, 1948] ($\theta_{cr,g} = 0.047$). A vegetation patch of length $L_{veg} = 500 \text{ m}$, comprising above- and below-ground vegetation, is placed between the coordinates $x_{up} = 600 \text{ m}$ and $x_{dw} = 1100 \text{ m}$ (Figure 2a) covering the entire channel width. We design this configuration to represent reach-scale morphodynamics of a vegetated gravel bar in a simplified way, as similarly done by previous experimental studies on sand-bed substrates [e.g. *Manners et al.*, 2015; *Diehl et al.*, 2017; *Le Bouteiller and Venditti*, 2014; *Le Bouteiller and Venditti*, 2015]. We mimic different types of vegetation depending on their impact on global flow resistance ($K_{s,v}$ in Table 1), while for the bare riverbed we use $K_{s,g} = 30 \text{ m}^{1/3} \text{ s}^{-1}$. The bottom stress reduction coefficient, γ , has been chosen within the range reported in *Vargas-Luna et al.* [2015]. Model runs are grouped into five sets based on the type of roots characterizing the patch. The control set *NR* has no roots. In sets *SR1* and *SR2*, we consider shallow- (Figure 1a) and deep-root distributions (Figure 1b) with different rooting depths, respectively. These root configurations are typically observed in field and laboratory experiments with cuttings and juvenile riparian vegetation growing in GBRs [e.g. *Pasquale et al.*, 2012; *Gorla et al.*, 2015]. The parameter values used in the root model are reported in the supporting information. For all simulations we set $\beta = 0.9$ in equation 5.

The numerical domain consists of cross-sections that are spaced out evenly (2 m) and vertical root distributions discretized by using riverbed layers of 0.1 m . For all runs, initial conditions are obtained by setting uniform flow conditions both at the inlet and the outlet of the numerical domain and by running fixed-bed simulation until the steady state is reached. Different water surface profiles are obtained for different values of $K_{s,v}$ and S_0 . We then perform morphodynamic simulations for the five sets until riverbed equilibrium is reached (at $t = T_{eq}$), keeping z_b fixed both at the inlet and outlet. The key parameter settings and configurations considered are summarized in Table 1.

Table 1. Model parameters defining numerical runs^a

Run	S_0	F_r	$K_{s,v}$	γ	$\theta_{cr,v}$	S_{eq}	E_{eq}	ζ_{upr}	ζ_r	Plant root type
	[–]	[–]	[$m^{1/3}s^{-1}$]	[–]	[m]	[–]	[m]	[m]	[m]	
NR-EP1	0.005	0.8	25	0.69	$\theta_{cr,g}$	0.0063	0.31	-	-	No roots
NR-EP2	0.005	0.8	20	0.44	$\theta_{cr,g}$	0.008	0.75	-	-	No roots
NR-EP3	0.02	1.5	25	0.69	$\theta_{cr,g}$	0.025	1	-	-	No roots
NR-EP4	0.005	0.8	15	0.25	$\theta_{cr,g}$	0.01	1.3	-	-	No roots
NR-EP5	0.02	1.5	15	0.25	$\theta_{cr,g}$	0.039	3.9	-	-	No roots
SR1-EP1	0.005	0.8	25	0.69	$[\theta_{cr,g}, 0.1, 0.2]$	-	0.31	0.45	0.6	Shallow
SR1-EP2	0.005	0.8	20	0.44	$[\theta_{cr,g}, 0.1, 0.2]$	-	0.75	0.45	0.6	Shallow
SR1-EP3	0.02	1.5	25	0.69	$[\theta_{cr,g}, 0.1, 0.2]$	-	1	0.45	0.6	Shallow
SR1-EP4	0.005	0.8	15	0.25	$[\theta_{cr,g}, 0.1, 0.2]$	-	1.3	0.45	0.6	Shallow
SR1-EP5	0.02	1.5	15	0.25	$[\theta_{cr,g}, 0.1, 0.2]$	-	3.9	0.45	0.6	Shallow
SR2-EP1	0.005	0.8	25	0.69	$[\theta_{cr,g}, 0.1, 0.2]$	-	0.31	0.55	0.8	Shallow
SR2-EP2	0.005	0.8	20	0.44	$[\theta_{cr,g}, 0.1, 0.2]$	-	0.75	0.55	0.8	Shallow
SR2-EP3	0.02	1.5	25	0.69	$[\theta_{cr,g}, 0.1, 0.2]$	-	1	0.55	0.8	Shallow
SR2-EP4	0.005	0.8	15	0.25	$[\theta_{cr,g}, 0.1, 0.2]$	-	1.3	0.55	0.8	Shallow
SR2-EP5	0.02	1.5	15	0.25	$[\theta_{cr,g}, 0.1, 0.2]$	-	3.9	0.55	0.8	Shallow
DR3-EP1	0.005	0.8	25	0.69	$[\theta_{cr,g}, 0.1, 0.2]$	-	0.31	0.75	0.8	Deep
DR3-EP2	0.005	0.8	20	0.44	$[\theta_{cr,g}, 0.1, 0.2]$	-	0.75	0.75	0.8	Deep
DR3-EP3	0.02	1.5	25	0.69	$[\theta_{cr,g}, 0.1, 0.2]$	-	1	0.75	0.8	Deep
DR3-EP4	0.005	0.8	15	0.25	$[\theta_{cr,g}, 0.1, 0.2]$	-	1.3	0.75	0.8	Deep
DR3-EP5	0.02	1.5	15	0.25	$[\theta_{cr,g}, 0.1, 0.2]$	-	3.9	0.75	0.8	Deep
DR4-EP1	0.005	0.8	25	0.69	$[\theta_{cr,g}, 0.1, 0.2]$	-	0.31	0.95	1	Deep
DR4-EP2	0.005	0.8	20	0.44	$[\theta_{cr,g}, 0.1, 0.2]$	-	0.75	0.95	1	Deep
DR4-EP3	0.02	1.5	25	0.69	$[\theta_{cr,g}, 0.1, 0.2]$	-	1	0.95	1	Deep
DR4-EP4	0.005	0.8	15	0.25	$[\theta_{cr,g}, 0.1, 0.2]$	-	1.3	0.95	1	Deep
DR4-EP5	0.02	1.5	15	0.25	$[\theta_{cr,g}, 0.1, 0.2]$	-	3.9	0.95	1	Deep

^a S_0 = initial riverbed slope, S_{eq} = equilibrium riverbed slope (only for runs NR), F_r = Froude number of the uniform flow, E_{eq} = erosion potential, $K_{s,v}$ = Strickler friction coefficient incorporating the effect of the drag generated by the vegetation γ = bottom stress reduction coefficient, $\theta_{cr,v}$ = critical Shields parameter incorporating the increase of cohesion due to the presence of roots, ζ_{upr} = riverbed depth at which uprooting occurs and ζ_r = rooting depth.

3 Results

3.1 The Role of Above-ground Vegetation

Numerical results from runs with no roots, in which we varied the roughness of the above-ground vegetation and the flow characteristics (set NR in Table 1), quantify the riverbed changes due to the interactions between flow and above-ground biomass. The final riverbed equilibrium (Figure 2b), which is common to all runs NR (Table 1), is characterized by an increased riverbed slope within the vegetated patch, a deposition in the upstream part, and a scour at x_{dw} (Figure 2b). Riverbed evolution starts with a deposition process from upstream the patch and erosion downstream ($t=0.05 T_{eq}$) (dash-dotted line in Figure 2c). Over time, while deposition advances downstream within the patch, erosion proceeds upstream ($t=0.1 T_{eq}$) (dashed lines in Figure 2c), progressively increasing the riverbed slope across the whole vegetated patch. The maximum bed level changes in our experiments occur at the interface between the vegetated and bare riverbed (at $x = \{x_{up}, x_{dw}\}$, Figure 2c). Riverbed steepening in vegetated areas has been previously reported [Le Bouteiller and Venditti, 2015]. Such configurations are a direct consequence of the friction exerted by the vegetation and the consequent reduction of the bed shear stress. Simulated flow velocities and bed shear stresses are reduced within and upstream from the vegetated patch. In addition, vegetation obstructs the flow increasing flow velocity and bed shear stress downstream from the patch. This, in turn, reduces the sediment transport capacity, q_b , within the vegetated patch, generating a sediment transport imbalance throughout the channel [Le Bouteiller and Venditti, 2014]. At equilibrium, the slope within the patch, S_{eq} (Table 1 and Figure 2b), depends on the difference between $K_{s,v}$ and $K_{s,g}$ and on flow characteristics (measured through the Froude number). We measure the strength of the erosion process, resulting from the interaction between flow and above-ground vegetation, through the *erosion potential* E_{eq} , i.e. the maximum scour at $x = x_{dw}$. Numerical runs of set NR give five different values of E_{eq} which are reported, in increasing order from EP1 to EP5, in Table 1.

3.2 The Role of Uprooting

Uprooting should play a fundamental role in the riverbed's response to erosion processes and deep roots by offering more anchoring resistance than shallow roots to erosional events. In addition, a sufficiently intense erosional event could completely remove

vegetation, regardless of the root distribution type. To test these hypotheses, we perform simulations of the sets SR and DR assuming $\theta_{cr,v} = \theta_{cr,g}$ (see Table 1) and leaving out the root-enhanced riverbed cohesion effect. Despite the presence of shallow (run SR2-EP4) or deep (run DR3-EP4) roots, bed evolution follows the same dynamics as the case with no roots (NR-EP4, Figure 2c) as long as the erosion at x_{dw} is smaller than ζ_{upr} (compare solutions at $t=0.05 T_{eq}$ in Figures 2d-e). If riverbed changes exceed ζ_{upr} , uprooting triggers an upward cascade-like mechanism that converts part of the vegetated patch to bare riverbed (Figures 2d-e). The erosion process stops when sediment balance is reached throughout the entire channel.

For a given erosion potential (EP4 in Figures 3a and 3b), uprooting leads to shorter patch lengths that are higher for shallow root profiles (runs SR2-EP4 and DR3-EP4 in Figure 3b). The time-to-uprooting is shorter for shallow roots (Figure 3b), since smaller scour depths, and therefore shorter times, are required to remove vegetation with shallow roots. In order to characterize the cumulative riverbed dynamics, in Figure 3a, we plot the time evolution of the integral of the normalized net eroded/deposited volume throughout the whole channel (V_{sed}). Compared to the case with no roots (run NR-EP4), the reduction of the patch length causes significant morphological changes while small differences are observed at equilibrium between shallow and deep root distributions.

The ratio between L_{veg} reached at equilibrium and its initial value ($L_{veg}(t_0)$) is shown for all the runs from series EP2 to EP5 in Figure 3c. Each line corresponds to runs characterized by the same erosion potential but different root distributions and therefore different ζ_{upr} . Results show that, for a given ζ_{upr} , the residual biomass (i.e. length of the patch at equilibrium) decreases as the strength of the erosion process increases (from EP2 to EP5). Shallow roots (small ζ_{upr}) (sets SR1 and SR2) lead to a residual biomass smaller than 0.4, regardless of the strength of the erosion process, whereas the length of deep rooted patches (sets DR3 and DR4) ranges between 0.05 and 1. Moreover, large values of the erosion potential result in shorter vegetated patches, smaller differences between shallow and deep roots (Figure 3c) and smaller deposition $V_{sed,up}$ upstream from the patch (black solid line in Figure 3d). As an example, in runs EP5, the vegetated patch is reduced by about 95% and $V_{sed,up}$ remains around 10% regardless of the root distribution type.

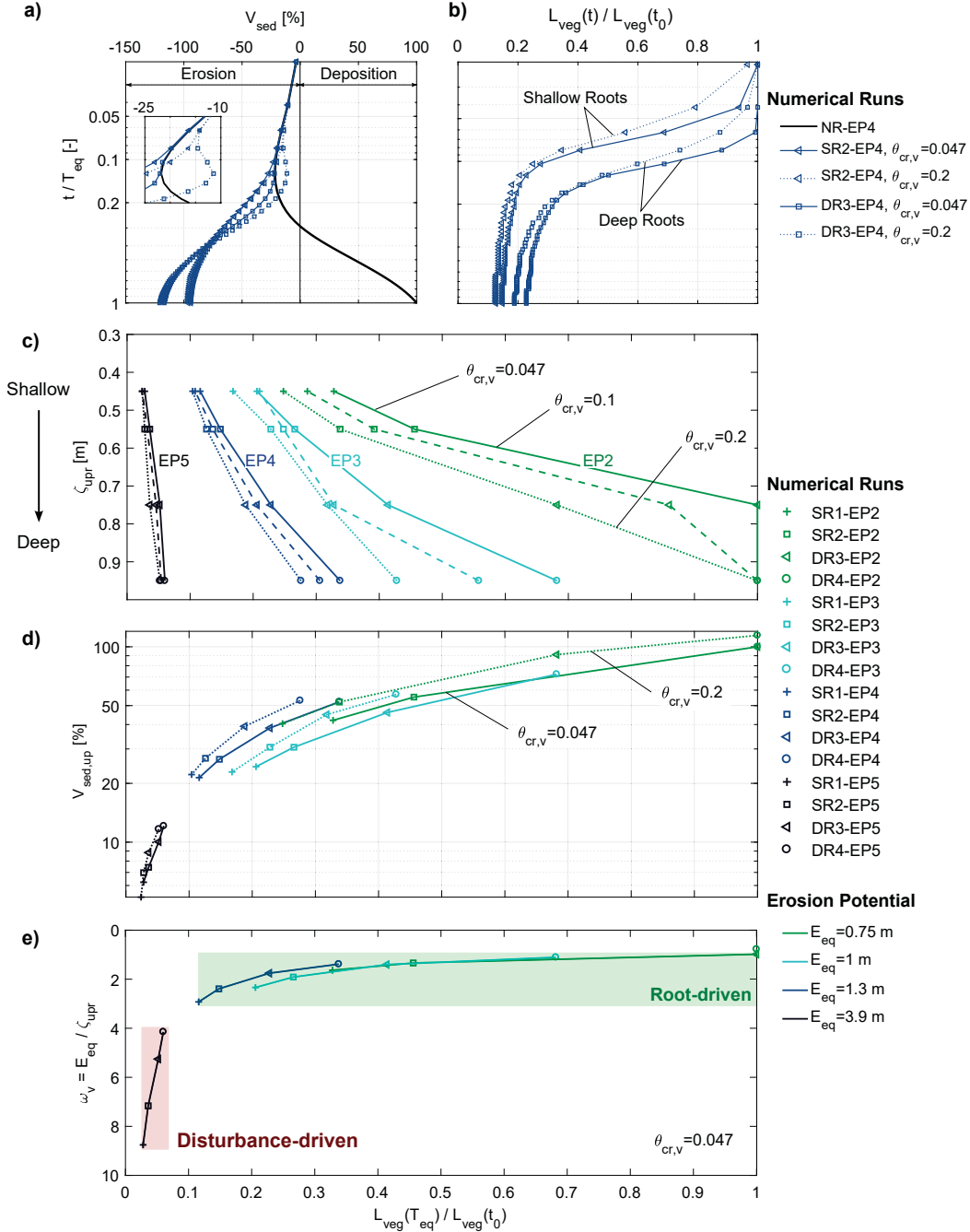


Figure 3. Plant-root controls on GBR morphodynamics. Time evolution of (a) normalized net

eroded/deposited volume along the channel, V_{sed} (%), and (b) normalized length of the vegetated patch

for shallow (SR2-EP4) and deep (DR3-EP4) roots. (c) Uprooting depth vs residual biomass. (d) Upstream

normalized deposited volume, $V_{sed,up}$ (%), versus residual biomass. (e) Influence of the relative strength

of erosion process, ω_v (equation 6), on the residual biomass. In all plots, solid lines refer to $\theta_{cr,v}=\theta_{cr,g}$,

while dashed and dotted lines to $\theta_{cr,v}=0.1$ and 0.2 , respectively. For a given run, the normalized net

eroded/deposited volume through the whole channel is calculated as $V_{sed} = \int_0^L \Delta z_b(t, x) / \Delta z_b^{NR}(t =$

$T_{eq}, x) dx$, where Δz_b^{NR} refers to the same run with no roots. $V_{sed,up}$ is calculated as V_{sed} but in the range

$x \in [0, x_{up}]$.

3.3 The Role of Root-enhanced Riverbed Cohesion

We investigate the effect of the root-enhanced riverbed cohesion by running simulations of sets SR and DR and considering $\theta_{cr,v} > \theta_{cr,g}$ (see Table 1). Root-enhanced cohesion affects riverbed dynamics only slightly (compare dashed and dotted lines vs solid lines in Figures 3a, 3c and 3d). Furthermore, it decreases the time-to-uprooting (see an example in Figure 3b), which reduces the length of the vegetated patch at equilibrium (Figure 3c). Such reduction is larger for deep roots and smaller for large values of E_{eq} (Figure 3c) and can be explained as follows. The added cohesion, i.e. higher critical shear stress, reduces sediment mobility and further decreases the transport capacity within the patch, which was already diminished by the above-ground effect of the vegetated patch. This causes a larger difference in transport capacity and hence an increase of the scour at the interface between the vegetated patch and the bare riverbed (see Figure S4 and Table S1), which in turn favors uprooting.

4 Discussion and Implications

Our modeling study demonstrates that the competition between the potential flow erosion and the uprooting depth mediates plant-root controls on GBR morphodynamics. The results of numerical runs show that the strength of the erosion process is primarily the result of the interactions between flow and above-ground vegetation, while vegetation anchoring resistance depends on the vertical root distribution. This competition can be measured by introducing the nondimensional parameter ω_v (a similar parameter has been previously used by *Perona and Crouzy* [2018]) defined as:

$$\omega_v = \frac{E_{eq}}{\zeta_{upr}} = \frac{\text{Strength of Erosion}}{\text{Vegetation Anchoring Resistance}} \quad , \quad (6)$$

where the strength of the erosion process is measured through the erosion potential, E_{eq} , representing the maximum erosion occurring in absence of any resisting force. Conversely, the resistance opposed by vegetation to uprooting is measured through the depth ζ_{upr} . If we plot ω_v against the normalized vegetated patch length, two different regions can be identified in Figure 3e: disturbance-driven and root-driven. Our results indicate that for $1 < \omega_v < 4$ (root-driven region) riverbed dynamics greatly depends on ω_v , whereas, for $\omega_v > 4$ (disturbance-driven region), changes in ω_v only slightly influence the length of the vegetated patch. The extension of these two regions is primarily controlled by the uprooting mechanism and is marginally affected by the root-enhanced riverbed cohesion.

Changes in the erosion rate might also influence the threshold values defining these regions [Perona and Crouzy, 2018]. In analogy to the nondimensional parameter, T^* , proposed by Tal and Paola [2007], defined as the ratio between characteristic timescales of riverbed reworking and vegetation encroachment, ω_v can provide information about morphological trajectories and may offers insights on the role played by the above- and below-ground vegetation components. For instance, in the disturbance-driven region, where erosional processes dominate, the riverbed will likely evolve towards a configuration with low vegetation cover and high sediment mobility, marginally affected by the root distribution. On the contrary, in the root-driven region ($E_{eq} \sim \zeta_{upr}$), erosion and plant anchoring resistance are balanced, producing conditions more suitable for vegetation development. In this region, the type of root distribution (deep or shallow), as well as plant canopy characteristics, can play a fundamental role in mediating the evolution of GBRs. Deep groundwater environments could favor the development of deep roots (Figure 1b) [Bertoldi *et al.*, 2011; Bätz *et al.*, 2016], which would enhance vegetation resistance to uprooting [Bywater-Reyes *et al.*, 2015]. Whereas, shallow and highly variable water tables (Figure 1a) may limit rooting depths and favor vegetation less resistant to erosional events [Tron *et al.*, 2014; Pasquale *et al.*, 2012]. The novelty of this model is the ability to take into account different environmental conditions, such as changes in water table dynamics, that can help interpreting observed vegetation-morphology dynamics [Bertoldi *et al.*, 2011; Bätz *et al.*, 2016].

In this study we explore simplified conditions to reduce the inherent complexity of the problem and disentangle the contribution of each feedback, independently. We examine the morphodynamics of a straight cohesionless gravel channel covered by a vegetation patch. This configuration does not target to capture vegetation dynamics and the associated development of fluvial landform over time [Gurnell, 2014], but rather to investigate the underlying processes occurring in GBRs at the event scale. However, the condition analyzed simplifies the topography of a real river gravel bar. The modeling framework we developed can be easily extended to take into account both flow unsteadiness and more complex morphologies, such as alternate bar patterns [Serlet *et al.*, 2018]. Moreover, we could investigate erosion processes related to changes in sediment supply rate [Gran *et al.*, 2015; Diehl *et al.*, 2017] and bar migration [Bertoldi *et al.*, 2014], which are not considered here. These processes might change the strength of erosion (i.e. E_{eq}) and thus the value of ω_v , possibly shifting a system from one region to another of Figure 3e. We use

a rather simple treatment of canopy effect on flow and sediment transport. For instance, local effects on scour and deposition pattern resulting from alteration of turbulence structures around vegetation patches can not be captured by the model [e.g. *Kim et al.*, 2015]. However, the model qualitatively captures the key features of riverbed adjustment in presence of vegetated patch observed in laboratory experiments [*Le Bouteiller and Venditti*, 2014; *Diehl et al.*, 2017].

The present results can have significant implications on the prediction of the co-evolution between vegetation and river morphology. Firstly, they suggest that a detailed description of uprooting in eco-morphodynamic models [*Solari et al.*, 2016] is a key ingredient needed for quantification. This is crucial for determining the effect of flood events on vegetation survival and development and on planning sustainable strategies for river restoration projects [e.g. *Bankhead et al.*, 2017; *Vesipa et al.*, 2017]. Secondly, model results suggest that further investigations linking plant roots, groundwater and river morphology are necessary. The proposed modeling framework can be extended to include above- and below-ground vegetation dynamics to predict morphological trajectories in relation to changes in water table dynamics. How vegetation allocates biomass to its above- and below-ground component might play a fundamental role on mediating biogeomorphic feedbacks. Finally, further investigations should examine the role of natural stochasticity of uprooting [*Perona and Crouzy*, 2018], which could be introduced by a stochastic representation of the critical root biomass (defined by β in our model).

Acknowledgments

We wish to thank W. Bertoldi for helpful discussions and for commenting the manuscript. The support of the Swiss National Science Foundation (Grant No. 159813) is gratefully acknowledged. We would like also to thank the Editor V. Yvanov and two anonymous reviewers for their constructive comments that greatly improved the manuscript. The numerical model BASEMENT can be freely downloaded at <http://www.basement.ethz.ch>. The results of numerical simulations used in the paper can be found at <https://polybox.ethz.ch/index.php/s/dcewDQq6KH36jj>.

References

Aberle, J., and J. Järvelä (2015), Hydrodynamics of vegetated channels, in *Rivers—Physical, Fluvial and Environmental Processes*, pp. 519–541, Springer.

- Bankhead, N. L., R. E. Thomas, and A. Simon (2017), A combined field, laboratory and numerical study of the forces applied to, and the potential for removal of, bar top vegetation in a braided river, *Earth Surface Processes and Landforms*, 42(3), 439–459, doi:10.1002/esp.3997.
- Bätz, N., P. Colombini, P. Cherubini, and S. N. Lane (2016), Groundwater controls on biogeomorphic succession and river channel morphodynamics, *Journal of Geophysical Research F: Earth Surface*, 121(10), 1763–1785, doi:10.1002/2016JF004009.
- Bertagni, M., C. Camporeale, and P. Perona (2018), Parametric transitions between bare and vegetated states in water-driven patterns, *Proceedings of the National Academy of Sciences*, doi:10.1073/pnas.1721765115.
- Bertoldi, W., N. A. Drake, and A. M. Gurnell (2011), Interactions between river flows and colonizing vegetation on a braided river: exploring spatial and temporal dynamics in riparian vegetation cover using satellite data, *Earth Surface Processes and Landforms*, 36(11), 1474–1486, doi:10.1002/esp.2166.
- Bertoldi, W., A. Siviglia, S. Tettamanti, M. Toffolon, D. Vetsch, and S. Francalanci (2014), Modeling vegetation controls on fluvial morphological trajectories, *Geophysical Research Letters*, 41(20), 7167–7175, doi:10.1002/2014GL061666.
- Bywater-Reyes, S., Andrew C. Wilcox, J. C. Stella, and A. F. Lightbody (2015), Flow and scour constraints on uprooting of pioneer woody seedlings, *Water Resources Research*, pp. 2760–2772, doi:10.1002/2014WR016632.Received.
- Cancienne, R. M., G. A. Fox, and S. Andrew (2008), Influence of seepage undercutting on the stability of root-reinforced streambanks, *Earth Surface Processes and Landforms*, 33(11), 1769–1786, doi:10.1002/esp.1657.
- Cardenas, M. B., J. Wilson, and V. A. Zlotnik (2004), Impact of heterogeneity, bed forms, and stream curvature on subchannel hyporheic exchange, *Water Resources Research*, 40(8).
- Corenblit, D., E. Tabacchi, J. Steiger, and A. M. Gurnell (2007), Reciprocal interactions and adjustments between fluvial landforms and vegetation dynamics in river corridors: A review of complementary approaches, *Earth-Science Reviews*, 84(1-2), 56–86, doi:10.1016/j.earscirev.2007.05.004.
- Corenblit, D., A. Baas, T. Balke, T. Bouma, F. Fromard, V. Garófano-Gómez, E. González, A. M. Gurnell, B. Hortobágyi, F. Julien, et al. (2015), Engineer pioneer plants respond to and affect geomorphic constraints similarly along water–terrestrial in-

- 421 interfaces world-wide, *Global Ecology and Biogeography*, 24(12), 1363–1376.
- 422 Davies, N. S., and M. R. Gibling (2011), Evolution of fixed-channel alluvial plains
- 423 in response to Carboniferous vegetation, *Nature Geoscience*, 4(9), 629–633, doi:
- 424 10.1038/ngeo1237.
- 425 Diehl, R. M., A. C. Wilcox, J. C. Stella, L. Kui, L. S. Sklar, and A. Lightbody (2017),
- 426 Fluvial sediment supply and pioneer woody seedlings as a control on bar-surface topog-
- 427 raphy, *Earth Surface Processes and Landforms*, 42(5), 724–734, doi:10.1002/esp.4017.
- 428 Edmaier, K., P. Burlando, and P. Perona (2011), Mechanisms of vegetation uprooting by
- 429 flow in alluvial non-cohesive sediment, *Hydrology and Earth System Sciences*, 15(5),
- 430 1615–1627, doi:10.5194/hess-15-1615-2011.
- 431 Edmaier, K., B. Crouzy, and P. Perona (2015), Experimental characterization of vegeta-
- 432 tion uprooting by flow, *Journal of Geophysical Research: Biogeosciences*, 120(9), 1812–
- 433 1824.
- 434 Fan, Y., G. Miguez-Macho, E. G. Jobbágy, R. B. Jackson, and C. Otero-Casal (2017), Hy-
- 435 drologic regulation of plant rooting depth, *Proceedings of the National Academy of Sci-*
- 436 *ences*, p. 201712381.
- 437 Gibling, M. R., and N. S. Davies (2012), Palaeozoic landscapes shaped by plant evolution,
- 438 *Nature Geoscience*, 5(2), 99–105, doi:10.1038/ngeo1376.
- 439 Gorla, L., C. Signarbieux, P. Turberg, A. Buttler, and P. Perona (2015), Transient response
- 440 of salix cuttings to changing water level regimes, *Water Resources Research*, 51(3),
- 441 1758–1774.
- 442 Gran, K. B., M. Tal, and E. D. Wartman (2015), Co-evolution of riparian vegetation and
- 443 channel dynamics in an aggrading braided river system, mount pinatubo, philippines,
- 444 *Earth Surface Processes and Landforms*, 40(8), 1101–1115, doi:10.1002/esp.3699.
- 445 Gregory, P. J. (2008), *Plant roots: growth, activity and interactions with the soil*, John Wi-
- 446 ley & Sons.
- 447 Gurnell, A. (2014), Plants as river system engineers, *Earth Surface Processes and Land-*
- 448 *forms*, 39(1), 4–25.
- 449 Gurnell, A. M., W. Bertoldi, and D. Corenblit (2012), Changing river channels: The
- 450 roles of hydrological processes, plants and pioneer fluvial landforms in humid tem-
- 451 perate, mixed load, gravel bed rivers, *Earth-Science Reviews*, 111(1), 129 – 141, doi:
- 452 <https://doi.org/10.1016/j.earscirev.2011.11.005>.

- 453 Jackson, R. B., J. Canadell, J. R. Ehleringer, H. A. Mooney, O. E. Sala, and E. D. Schulze
454 (1996), A global analysis of root distributions for terrestrial biomes, *Oecologia*, 108(3),
455 389–411, doi:10.1007/BF00333714.
- 456 Kim, H. S., I. Kimura, and Y. Shimizu (2015), Bed morphological changes around a fi-
457 nite patch of vegetation, *Earth Surface Processes and Landforms*, 40(3), 375–388, doi:
458 10.1002/esp.3639, eSP-13-0354.R3.
- 459 Kim, J., V. Y. Ivanov, and N. D. Katopodes (2012), Hydraulic resistance to overland flow
460 on surfaces with partially submerged vegetation, *Water Resources Research*, 48(10).
- 461 Le Bouteiller, C., and J. Venditti (2015), Sediment transport and shear stress partitioning
462 in a vegetated flow, *Water Resources Research*, 51(4), 2901–2922.
- 463 Le Bouteiller, C., and J. G. Venditti (2014), Vegetation-driven morphodynamic ad-
464 justments of a sand bed, *Geophysical Research Letters*, 41(11), 3876–3883, doi:
465 10.1002/2014GL060155.
- 466 Manners, R. B., A. C. Wilcox, L. Kui, A. F. Lightbody, J. C. Stella, and L. S. Sklar
467 (2015), When do plants modify fluvial processes? Plant-hydraulic interactions under
468 variable flow and sediment supply rates, *Journal of Geophysical Research: Earth Sur-
469 face*, 120(2), 325–345.
- 470 Meyer-Peter, E., and R. Müller (1948), Formulas for bed-load transport, in *2nd Meeting*,
471 *Int. Assoc. of Hydraul. Eng. and Res.*, Stockholm.
- 472 Murray, A. B., and C. Paola (2003), Modelling the effect of vegetation on channel pattern
473 in bedload rivers, *Earth Surface Processes and Landforms*, 28(2), 131–143.
- 474 Nardin, W., and D. A. Edmonds (2014), Optimum vegetation height and density for inor-
475 ganic sedimentation in deltaic marshes, *Nature Geoscience*, 7(10), 722.
- 476 Nepf, H. M. (2012), Flow and Transport in Regions with Aquatic Vegetation, *Annual Re-
477 view of Fluid Mechanics*, 44(1), 123–142, doi:10.1146/annurev-fluid-120710-101048.
- 478 Oorschot, M. v., M. Kleinans, G. Geerling, and H. Middelkoop (2016), Distinct patterns
479 of interaction between vegetation and morphodynamics, *Earth Surface Processes and
480 Landforms*, 41(6), 791–808.
- 481 Orellana, F., P. Verma, S. P. Loheide, and E. Daly (2012), Monitoring and modeling
482 water-vegetation interactions in groundwater-dependent ecosystems, *Reviews of Geo-
483 physics*, 50(3).
- 484 Pasquale, N., and P. Perona (2014), Experimental assessment of riverbed sediment rein-
485 forcement by vegetation roots, *River Flow 2014*, pp. 553–561.

- 486 Pasquale, N., P. Perona, R. Francis, and P. Burlando (2012), Effects of streamflow variabil-
487 ity on the vertical root density distribution of willow cutting experiments, *Ecological*
488 *Engineering*, 40, 167–172, doi:10.1016/j.ecoleng.2011.12.002.
- 489 Perona, P., and B. Crouzy (2018), Resilience of riverbed vegetation to uprooting by flow,
490 *Proceedings of the Royal Society A: Mathematical, Physical and Engineering Sciences*.
- 491 Politti, E., W. Bertoldi, A. Gurnell, and A. Henshaw (2018), Feedbacks between the ri-
492 parian salicaceae and hydrogeomorphic processes: A quantitative review, *Earth-Science*
493 *Reviews*, 176, 147 – 165, doi:https://doi.org/10.1016/j.earscirev.2017.07.018.
- 494 Pollen-Bankhead, N., and A. Simon (2010), Hydrologic and hydraulic effects of ripar-
495 ian root networks on streambank stability: Is mechanical root-reinforcement the whole
496 story?, *Geomorphology*, 116(3-4), 353–362.
- 497 Polvi, L. E., E. Wohl, and D. M. Merritt (2014), Modeling the functional influence of veg-
498 etation type on streambank cohesion, *Earth Surface Processes and Landforms*, 39(9),
499 1245–1258, doi:10.1002/esp.3577.
- 500 Ridolfi, L., P. D’Odorico, and F. Laio (2011), *Noise-induced phenomena in the*
501 *environmental sciences*, xii, 313 p. pp., Cambridge University Press, doi:
502 10.1017/CBO9780511984730.
- 503 Schwarz, C., O. Gourgue, J. van Belzen, Z. Zhu, T. J. Buoma, J. van de Koppel,
504 G. Ruessink, N. Claude, and S. Temmerman (2018), Self-organization of a biogeomor-
505 phic landscape controlled by plant life-history traits, *Nature Geoscience*.
- 506 Serlet, A. J., A. M. Gurnell, G. Zolezzi, G. Wharton, P. Belleudy, and C. Jourdain (2018),
507 Biomorphodynamics of alternate bars in a channelized, regulated river: an integrated
508 historical and modelling analysis, *Earth Surface Processes and Landforms*.
- 509 Simon, A., and A. J. C. Collison (2001), Pore-water pressure effects on the detachment of
510 cohesive streambeds: seepage forces and matric suction, *Earth Surface Processes and*
511 *Landforms*, 26(13), 1421–1442, doi:10.1002/esp.287.
- 512 Solari, L., M. Van Oorschot, B. Belletti, D. Hendriks, M. Rinaldi, and A. Vargas-Luna
513 (2016), Advances on modelling riparian vegetation-hydromorphology interactions, *River*
514 *Research and Applications*, 32(2), 164–178.
- 515 Tal, M., and C. Paola (2007), Dynamic single-thread channels maintained by the interac-
516 tion of flow and vegetation, *Geology*, 35(4), 347, doi:10.1130/G23260A.1.
- 517 Tal, M., and C. Paola (2010), Effects of vegetation on channel morphodynamics: results
518 and insights from laboratory experiments, *Earth Surface Processes and Landforms*,

- 519 35(9), 1014–1028, doi:10.1002/esp.1908.
- 520 Temmerman, S., T. Bouma, J. Van de Koppel, D. Van der Wal, M. De Vries, and P. Her-
 521 man (2007), Vegetation causes channel erosion in a tidal landscape, *Geology*, 35(7),
 522 631, doi:10.1130/G23502A.1.
- 523 Tron, S., F. Laio, and L. Ridolfi (2014), Effect of water table fluctuations on phreato-
 524 phytic root distribution, *Journal of Theoretical Biology*, 360, 102–108, doi:
 525 10.1016/j.jtbi.2014.06.035.
- 526 Tron, S., P. Perona, L. Gorla, M. Schwarz, F. Laio, and L. Ridolfi (2015), The signature
 527 of randomness in riparian plant root distributions, *Geophysical Research Letters*, 42(17),
 528 7098–7106, doi:10.1002/2015GL064857.
- 529 Vannoppen, W., M. Vanmaercke, S. De Baets, and J. Poesen (2015), A review of the me-
 530 chanical effects of plant roots on concentrated flow erosion rates, *Earth-Science Re-*
 531 *views*, 150, 666–678.
- 532 Vargas-Luna, A., A. Crosato, and W. S. Uijttewaai (2015), Effects of vegetation on flow
 533 and sediment transport: comparative analyses and validation of predicting models, *Earth*
 534 *Surface Processes and Landforms*, 40(2), 157–176.
- 535 Västilä, K., and J. Järvelä (2014), Modeling the flow resistance of woody vegetation using
 536 physically based properties of the foliage and stem, *Water Resources Research*, 50(1),
 537 229–245, doi:10.1002/2013WR013819.
- 538 Vesipa, R., C. Camporeale, and L. Ridolfi (2017), Effect of river flow fluctuations on
 539 riparian vegetation dynamics: processes and models, *Advances in Water Resources*,
 540 110(July), 29–50, doi:10.1016/j.advwatres.2017.09.028.
- 541 Vetsch, D., A. Siviglia, D. Ehrbar, M. Facchini, S. Kammerer, A. Koch, S. Peter, L. Von-
 542 willer, M. Gerber, C. Volz, D. Farshi, R. Mueller, P. Rousselot, R. Veprek, and R. Faeh
 543 (2017), *System Manuals of BASEMENT, Version 2.7*, Laboratory of Hydraulics, Glaciol-
 544 ogy and Hydrology (VAW). ETH Zurich.
- 545 Wohl, E., S. N. Lane, and A. C. Wilcox (2015), The science and practice of river restora-
 546 tion, *Water Resources Research*, 51(8), 5974–5997.
- 547 Yager, E., and M. Schmeeckle (2013), The influence of vegetation on turbulence and bed
 548 load transport, *Journal of Geophysical Research: Earth Surface*, 118(3), 1585–1601.